JPL Document No. D-xxxxx

CloudSat Project

A NASA Earth System Science Pathfinder Mission

Level 2C Snow Profile Process Description and Interface Control Document

Algorithm Version: P_R04

Document Version: 0.

Date: 10 February, 2013

Address questions concerning this document to:
Norman Wood
norman.wood@ssec.wisc.edu
608-265-3675

Approvals

_____Date_____
Norman Wood
Data Product Algorithm Lead

_____Date_____
Tristan L'Ecuyer
Data Product Algorithm Lead

_____Date_____
Deborah Vane
Deputy Project Scientist

_____Date_____
Graeme Stephens
Project Scientist

_____Date_____
Phil Partain
Data Processing Center Lead Engineer

Contents

1 Introduction

The CloudSat Snow Profile product (2C-SNOW-PROFILE) provides estimates of vertical profiles of snowfall rate along with snow size distribution parameters and snow water content for radar reflectivity profiles observed by the CloudSat Cloud Profiling Radar (CPR) which, based on an evaluation of the profile and ancillary data, appear to coincide with snow at the surface. For these profiles, the product also estimates snowfall rate at the surface. Because of ground clutter, the CPR cannot reliably measure reflectivities near the surface. To overcome this limitation, the product algorithm estimates snow properties using a truncated reflectivity profile, terminated somewhat above the surface, then uses the estimated snow properties in the bottom-most portion of the profile to estimate the surface snowfall rate. For the truncated reflectivity profile, profiles of size distribution parameters are retrieved using an optimal estimation algorithm which incorporates a priori information about snow microphysical properties, radar scattering properties, and size distribution parameters. Retrievals are performed only for profiles which appear likely to contain snow at the surface, either dry snow or snow with a small melted mass fraction. The retrieved size distribution parameter profiles and the a priori information are then used to calculate profiles of snowfall rates and snow water contents. The optimal estimation method produces uncertainty estimates for the retrieved size distribution parameters, and these uncertainties are then used to estimate uncertainties for the snowfall rates and snow water contents.

This document describes the algorithm that has been implemented in Release 4 (R04) of the 2C-SNOW-PROFILE product (algorithm version 0.). For each radar profile, the algorithm

- examines variables from 2C-PRECIP-COLUMN to determine if snowfall is present at the surface. In cases where the 2C-PRECIP-COLUMN data are inconclusive, the algorithm examines the near-surface reflectivities and cloud mask from 2B-GEOPROF and temperatures from ECMWF-AUX to determine if snowfall is present at the surface;
- examines the reflectivity and cloud mask profile from 2B-GEOPROF and the temperature profile from ECMWF-AUX to locate a snow layer: a near-surface, contiguous range of radar bins which contain snow;
- assigns a priori expected values, uncertainties and initial values to the snow size distribution parameters in each snow-containing radar bin in the snow layer;
- retrieves a profile of snow size distribution parameters and their uncertainties using the radar reflectivity profile in the snow layer;
- calculates a profile of snowfall rates, snow water contents and their uncertainties for the snow layer;
- and estimates the surface snowfall rate and its uncertainty using the snowfall rate and its uncertainty from the base of the snow layer.

2 Product Contents

The product is provided in HDF format, in files each of which contain both geolocation information and product data for a single orbit, or granule. Variables are dimensioned as scalars; as arrays of dimension N_{ray}, where N_{ray} is the number of vertical radar profiles measured during the orbit; or as arrays of dimension N_{bin} x N_{ray}, where N_{bin} is the number of vertical radar bins in a profile.

2.1 Data fields

Data fields are tabulated in Table 1 and, except as noted, are produced by 2C-SNOW-PROFILE. Descriptions of the fields provided by 2C-SNOW-PROFILE follow. For other fields, see the documentation of the referenced products.

Table 1: 2C-SNOW-PROFILE data fields.

Variable	Dimension	Units	Description
Data_quality	N_{ray}	–	Flags indicating radar data quality (from 2B-GEOPROF)
Data_status	N_{ray}	–	Spacecraft data status flags (from 2B-GEOPROF)
Data_targetID	N_{ray}	–	CPR bus orientation (from 2B-GEOPROF)
snow_retrieval_status	N_{ray}	–	Retrieval status flags (see description below)
norm_chi_sq	N_{ray}	–	Retrieval normalized chi square
log_N0	N_{bin},N_{ray}	$\log_{10}(m^{-3}\ mm^{-1})$	Log_{10} of the snow size distribution intercept parameter, N_0
log_N0_uncert	N_{bin},N_{ray}	$\log_{10}(m^{-3}\ mm^{-1})$	Uncertainty of $\log_{10}(N_0)$
log_lambda	N_{bin},N_{ray}	$\log_{10}(mm^{-1})$	Log_{10} of the snow size distribution slope parameter, λ
log_lambda_uncert	N_{bin},N_{ray}	$\log_{10}(mm^{-1})$	Uncertainty of $\log_{10}(\lambda)$
snowfall_rate	N_{bin},N_{ray}	$mm\ h^{-1}$	Snowfall rate profile, S
snowfall_rate_uncert	N_{bin},N_{ray}	$mm\ h^{-1}$	Uncertainty of S
snowfall_rate_sfc	N_{bin},N_{ray}	$mm\ h^{-1}$	Snowfall rate at the surface, S_{sfc}
snowfall_rate_sfc_uncert	N_{bin},N_{ray}	$mm\ h^{-1}$	Uncertainty in S_{sfc}
snowfall_rate_sfc_confidence	N_{bin},N_{ray}	–	Parameter indicating confidence in S_{sfc} (see description below)
snow_water_content	N_{bin},N_{ray}	$g\ m^{-3}$	Snow water content, SWC
snow_water_content_uncert	N_{bin},N_{ray}	$g\ m^{-3}$	Uncertainty in SWC

snow_retrieval_status The retrieval status for each profile is represented by an 8-bit field, stored in the HDF file as a signed, 1-byte integer value in variable snow_retrieval_status. The interpretation of each bit is as follows:

Bit 0: (Least significant bit) A snow layer is detected in the profile. Detection is based on a combined evaluation of the reflectivities, cloud mask values and temperatures in the truncated profile.

Bit 1: Snow is indicated at the surface. For most profiles, this is determined by examining the variables Precip_flag and Melted_fraction from 2C-PRECIP-COLUMN. This flag is set if Precip_flag indicates "Snow certain" or "Snow possible", or if it indicates "Mixed certain" or "Mixed possible" with a value of Melted_fraction less than or equal to 0.1. Additionally, if the 2C-PRECIP-COLUMN variables are not conclusive, 2C-SNOW-PROFILE performs an independent evaluation. If snow is detected in the truncated profile, and the temperatures at the surface are sufficiently cold so that the melted mass fraction is less than or equal to 0.1, snow is indicated at the surface.

Bit 2: A retrieval was performed, but produced large chi-square values. This can be an indication the retrieval has converged to a state that is inconsistent with the observations or with the a priori assumptions, and suggests the results should be used with caution.

Bit 3: The snowfall rate at the base of the snow layer is substantially larger than that in the profile bin immediately above. This may be an indication of the effects of surface clutter, shallow precipitation, or partial melting of the snow, and suggests these results should be used with caution. See section 8 for further details.

Bit 4: Inputs required from surface data are missing or in error. No retrieval is performed.

Bit 5: Inputs required from profile data are missing or in error. No retrieval is performed.

Bit 6: A retrieval was attempted and converged to invalid values.

Bit 7: (Most significant bit) A retrieval was attempted and failed to converge.

norm_chi_square This is the chi square value calculated for the retrieved state, divided by the number of observations (see section 4.2). Values larger than 1 may be an indication of improper convergence.

log_N0, log_N0_uncert The profile within the snow layer of the retrieved values of the $\log_{10}$-transformed intercept parameters of an assumed exponential snow particle size distribution (PSD), and their retrieved uncertainties.

log_lambda, log_lambda_uncert The profile within the snow layer of the retrieved values of the $\log_{10}$-transformed slope parameters of an assumed exponential snow particle size distribution (PSD), and their retrieved uncertainties.

snowall_rate, snowfall_rate_uncert The profile within the snow layer of snowfall rates calculated using the retrieved values of $\log_{10}(N_0)$ and $\log_{10}(\lambda)$, and the a priori model of snow microphysical properties. Uncertainties are calculated by propagating the retrieved uncertainties in $\log_{10}(N_0)$ and $\log_{10}(\lambda)$, and the estimated a priori uncertainties in the snow microphysical property model into the snowfall rate calculation.

snowfall_rate_sfc, snowfall_rate_sfc_uncert The estimated snowfall rate at the surface and its uncertainty. These are estimated as the snowfall rate and its uncertainty from the radar bin at the base of the snow layer.

snowfall_rate_sfc_confidence Confidence in the surface snowfall rate for each profile represented by an integer value interpreted as follows:

-1: No retrieval or failed retrieval.

0: No confidence.

1: Very low confidence.

2: Low confidence.

3: Moderate confidence.

4: High confidence.

Values are set as shown in Table 2. For profiles which appear to have dry snow at the surface, the initial value is set to 3 (moderate confidence). If the surface type (2C-PRECIP-COLUMN variable Surface_type) is other than "open ocean", the value is reduced by 1. If the snowfall rate at the base of the truncated profile is substantially larger than that in the profile bin immediately above (bit 3 of retrieval_status is set), the value is reduced by 1. Finally, the value is adjusted if multiple scattering and attenuation contribute substantial uncertainties to the modeled reflectivity at the base of the truncated profile. The adjusted value is limited to range between 0 (no confidence) and 4 (high confidence). For partially melted snow, the initial value is 1 (very low confidence), and no adjustments are applied.

Table 2: Settings for surface snowfall rate and its confidence value.

Surface Precip Type	melted mass fraction	snow layer/retrieval	Srate	confidence
Missing			missing	-1
None			0.	4
Rain			0.	4
Mixed	unknown		missing	-1
Mixed	(0.1, 1.0]		0.	1
Mixed	[0., 0.1]	absent/none	0.	0
“	“	present/failed	missing	-1
“	“	present/successful	per retrieval	1
“	“	unknown/none	missing	-1
Snow		absent/none	0.	0
“		present/failed	missing	-1
“		present/successful	per retrieval	3 + Mods
“		unknown/none	missing	-1

Table 3: Adjustments to the surface snowfall rate confidence value for forward model uncertainties due to multiple scattering and attenuation.

s(Ze), dBZe	Modifier
< 3	+1
3 - 6	0
6 - 12	-1
> 12	-2

snow_water_content, snow_water_content_uncert

The profile within the snow layer of snow water contents calculated using the retrieved values of $\log_{10}(N_0)$ and $\log_{10}(\lambda)$, and the a priori model of snow microphysical properties. Uncertainties are calculated by propagating the retrieved uncertainties in $\log_{10}(N_0)$ and $\log_{10}(\lambda)$, and the estimated a priori uncertainties in the snow microphysical property model in the snow water content calculation.

2.2 Geolocation fields

All geolocation information is passed through from 2B-GEOPROF (Table 4). See documentation for the 2B-GEOPROF product for further details.

Table 4: 2C-SNOW-PROFILE geolocation fields.

Variable	Dimension	Units	Description
Profile_time	N_{ray}	seconds	Seconds since the start of the granule for each profile
UTC_start	scalar	seconds	The UTC seconds since 00:00 UTC for the first profile in the granule
TAI_start	scalar	seconds	The International Atomic Time (seconds since 00:00:00 1 January 1993) for the first profile in the granule
Latitude	N_{ray}	degrees	Spacecraft geodetic latitude
Longitude	N_{ray}	degrees	Spacecraft geodetic longitude
Height	N_{bin},N_{ray}	m	Height of radar range bins above mean sea level
DEM_elevation	N_{ray}	m	Terrain elevation above mean sea level
Vertical_binsize	scalar	m	Effective vertical height of the radar range bins

3 Algorithm Theoretical Basis

Snowfall rate depends on the abundance of snow particles of different sizes (the particle size distribution, or PSD), the masses of those particles, and their fallspeeds. Fallspeeds in turn depend on particle masses, their shapes, and environmental conditions. As is true for lower-frequency precipitation radars, radar backscattering at the 94 GHz frequency used by the CPR is sensitive to PSD and particle masses; however, at this higher frequency, backscattering is also sensitive to particle shape. With even simple models for the PSD, the particle masses and the shapes, observations of 94 GHz radar reflectivity alone are insufficient to constrain the models sufficiently to determine snowfall rates. To address this insufficiency, optimal estimation is used as the retrieval method for 2C-SNOW-PROFILE. This method enables the use of explicit a priori information which can help constrain the retrievals. Additionally, optimal estimation allows uncertainties in the retrieval assumptions and observations to be propagated into estimates of uncertainties in retrieval products such as snowfall rate.

3.1 Radar reflectivity

At the frequencies used by cloud radars, scattering by precipitation-sized particles generally does not follow the Rayleigh approximation, and attenuation of the radar beam by hydrometeors and gases may be significant. Under these conditions and assuming single scattering, the effective radar reflectivity factor as a function of range from the radar is given by

$$Ze(R) = \frac{\Lambda^4}{\|K_w\|^2 \pi^5} \exp\left[-2\int_{s=0}^{s=R} \beta_{ext}(s)ds\right] \int_{D_{min}}^{D_{max}} N(D,R)\sigma_{bk}(D,R)dD \quad (1)$$

where R is the range, s is the position along the path of the beam, $\sigma_{bk}(D,R)$ is the backscatter cross-section for particle size D at range R, $N(D,R)$ is the size distribution at range R, Λ is the radar wavelength, $\|K_w\|^2$ is the dielectric factor for water, and $\beta_{ext}(s)$ is the volume extinction coefficient along the path of the radar beam. The exponential term is the two-way transmission between the radar and the observed radar volume at range R and represents losses in the transmitted and reflected power due to scattering and absorption along the path to the target.

The volume extinction coefficient includes contributions due to scattering and absorption by hydrometeors and due to absorption by gases, and is given by

$$\beta_{ext}(s) = \int_{D_{min}}^{D_{max}} N(D,s)\sigma_{ext}(D,s)dD + \sum_i k_{abs,i}(s)\rho_i(s) \quad (2)$$

where $N(D,s)$ is the hydrometeor size distribution at position s, $\sigma_{ext}(D,s)$ is the hydrometeor extinction cross-section, $k_{abs,i}(s)$ is the mass absorption coefficient for gas species i, and $\rho_i(s)$ is the corresponding gas density. At 94 GHz, gaseous attenuation is predominantly due to water vapor; the two-way attenuation by water vapor in tropical atmospheres can approach 5 dB (Stephens et al., 2002). The 2B-GEOPROF product provides estimates of the two-way gaseous attenuation, and the snowfall retrieval algorithm uses these estimates to correct the 2B-GEOPROF reflectivities before a retrieval is performed.

Attenuation by frozen hydrometeors may also be substantial; however, under heavier snow conditions for which attenuation is a factor, multiple scattering partially offsets the attenuation (Matrosov and Battaglia, 2009). This compensating behavior in heavy snow causes the multiply-scattered attenuated reflectivity to lie between the singly-scattered nonattenuated and singly-scattered attenuated reflectivities. The results of Matrosov and Battaglia show that both the singly-scattered attenuated and nonattenuated reflectivities are biased estimates of the multiply-scattered attenuated reflectivity. Absent an explicit multiple scattering model for heavy snow, the multiply-scattered attenuated reflectivity may be approximated using the singly-scattered attenuated and nonattenuated reflectivities as bounding values. Additionally, the uncertainties for this approximation can be estimated from the difference in the singly-scattered attenuated and nonattenuated reflectivities.

Liquid hydrometeors also produce attenuation. While the CloudSat snowfall retrieval will not be applied to profiles thought to contain liquid cloud and rain, supercooled liquid water may also attenuate the radar beam. A single-wavelength, nadir-pointing radar such as the CPR lacks means for identifying the presence of supercooled water. Future developments may allow for treatment of attenuation by supercooled liquid water in the retrieval; for this product, this attenuation is omitted.

3.2 Snowfall rate

The snowfall rate S at some range R in the radar profile in units of liquid water depth per unit time is

$$S(R) = \frac{1}{\rho_{liq}} \int_{D_{min}}^{D_{max}} N(D,R) m(D,R) V(D,R)\, dD, \tag{3}$$

where $m(D,R)$ is particle mass and$V(D,R)$ is fallspeed, and ρ_{liq} is the density of liquid water. Fallspeeds may be described using explicit, physically-based relations. As described by Mitchell (1996), the dimensionless Best, or Davies, number X relates the Reynolds number Re and drag coefficient C_d for a falling particle and is expressed in terms of the particle mass and the particle area projected normal to the direction of motion:

$$X(D) = C_d Re^2 = \frac{2D^2 \rho_a g}{\mu^2} \frac{m(D)}{A_p(D)}, \tag{4}$$

where $A_p(D)$ is the projected area of the particle, ρ_a is the air density, μ is the viscosity, and g is gravitational acceleration. Arguments based on boundary layer theory for blunt bodies (Abraham, 1970) give an expression for Re in terms of the Best number, which Mitchell and Heymsfield (2005) modified to account for the enhancement of boundary layer effects in porous snow aggregates:

$$Re(D) = \frac{\delta_0^2}{4} \left[\left(1 + \frac{4\sqrt{X(D)}}{\delta_0^2 \sqrt{C_0}} \right)^{1/2} - 1 \right]^2 - a_0 [X(D)]^{b_0}, \tag{5}$$

with a_0= 0.0017 and b_0=0.8 being parameters describing the enhanced boundary layer effects, δ_0 is a constant related to boundary layer thickness and C_0 is the limiting drag coefficient under conditions dominated by pressure drag. Finally, the fallspeed can be found as

$$V(D) = \frac{Re(D)\,\mu}{\rho_a D}. \tag{6}$$

Note that D appears explicitly in the expressions for $V(D)$ and $X(D)$, making them sensitive to the choice of D. For fallspeeds of nonspherical ice particles, D is taken typically to be the maximum dimension of the particle, D_M.

3.3 Particle model

The relationships described above require size-dependent particle properties including mass, horizontally-projected area, backscatter cross-sections, and extinction cross-sections. Particle masses and horizontally-projected areas are given by power laws (Locatelli and Hobbs, 1974; Mitchell, 1996)

$$m(D_M) = \alpha D_M^{\beta} \tag{7}$$

$$A_p(D_M) = \gamma D_M^{\sigma}. \tag{8}$$

For small particles, these relationships can produce masses which exceed those of ice spheres and areas which exceed those of circles, so for a given particle size D_M, particle mass is capped to be no greater than that of an ice sphere of the same diameter. Similarly, particle area is capped to be no more than that of a circle of the same diameter. Radar backscattering and extinction cross-sections are calculated via the discrete dipole approximation (Draine and Flatau, 1994), an approach suitable for irregularly-shaped particles.

Specifying the particle masses and areas partially constrain the dipole models needed to calculate scattering properties; however, additional assumptions must be made about particle shape. Additionally, the parameters α, β, γ, and σ vary depending on factors including particle habit and degree of riming. The limited information available in reflectivity measurements precludes these properties from being retrieved. Instead, best estimates and uncertainties for the parameters and scattering properties were obtained from analyses of single particle measurement and other in-situ and remote sensing observations of snow particles (Wood, 2011). Dipole models were constructed using shapes found to best reproduce observed 94-GHz reflectivity measurements from a cold-season validation experiment (the Canadian CloudSat CALIPSO Validation Project, C3VP, (Hudak et al., 2006). These a priori descriptions of particle properties constitute the particle model used by the algorithm

3.4 Size distribution

Given the particle model, the remaining term needed to determine radar reflectivity or snowfall rate is the snow particle size distribution. Distributions of snow particle sizes are frequently characterized as exponential

$$N(D) = N_0 \exp(-\lambda D) \tag{9}$$

where λ is the slope of the distribution and N_0 its intercept. While in general D may be either the melted drop diameter or an actual dimension of the particle, for 2C-SNOW-PROFILE an exponential form is used in which D is the maximum particle dimension, D_M.

Exponential behavior, especially at larger particle sizes, has been confirmed in aircraft-based in situ observations under a wide range of atmospheric conditions (Braham, 1990; Passarelli, 1978; Lo and Passarelli, 1982; Gordon and Marwitz, 1984; Houze et al., 1979; Woods et al., 2008) . Some studies of aircraft observations have noted departures from exponential behavior (e.g., "super-" or "sub-exponential", Herzegh and Hobbs, 1985). Heymsfield et al. (2008) examined the adequacy of exponential distributions for snow, looking at the ability of a fitted exponential distribution to reproduce ice water contents and Rayleigh reflectivities calculated directly from the binned particle size distributions. They found that parameters derived from higher moments of the particle size distribution, which are more directly related to ice water content and radar reflectivity, produced exponential distributions which generally provided good agreement with IWC and Ze values calculated from the observed, binned size distributions.

For observations at the surface, estimates of size distributions based on actual particle dimension D_M have been far less common. Rogers (1973) used photographs of snowflakes to develop estimates of snow size distributions based on actual dimensions and also found snow size distributions to be exponential. Brandes et al. (2007) evaluated both exponential and gamma forms, which have the ability to represent sub- or super-exponential behavior, for snow size distributions observed by a 2D video disdrometer over the course of several winter seasons. Although about 22% of the observed snow distributions exhibited super-exponential features, more commonly the fitted gamma distributions were nearly equivalent to exponential distributions.

4 Implementation

4.1 Scene Characterization

Scene characterization determines if snow is present in the radar profile and if the snow is reaching the surface without significant melting. Because ground clutter contaminates the radar reflectivities in the range bins nearest the surface, these two evaluations are done independently.

4.1.1 Near-surface bin

Before the profile is evaluated for the presence of snow, the clutter-contaminated range bins near the surface must be excluded. The number of excluded bins depends on the surface type. If the 2C-PRECIP-COLUMN variable Surface_type indicates the surface is ocean without sea ice, or inland water, the two range bins immediately above the surface-containing range bin are excluded. If the surface is identified as land, sea ice, or unknown, the four range bins immediately above the surface-containing range bin are excluded. This approach matches how 2C-PRECIP-COLUMN identifies the near-surface bin, the range bin that is nearest the surface and expected to be free of clutter.

4.1.2 Profile characterization

Starting from the near-surface bin and working upward, the profile is examined for significant radar returns. Significant returns are those which have a 2B-GEOPROF CPR_Cloud_mask value greater than or equal to 20. Consistent with 2C-PRECIP-COLUMN, CPR_Cloud_mask values of 5 are also not excluded. If a significant return is present in the near-surface bin at the base of the profile, the lowest contiguous layer of significant returns is denoted as a hydrometeor layer.

The characteristics of this hydrometeor layer are then evaluated. First the reflectivity profile is examined to determine if precipitation is present using a reflectivity threshold of -15 dBZe. This threshold is based on the identification of very light liquid precipitation at -10 dBZe in Ka-band radar observations by Stephens and Wood (2007) and the "Rain possible" and "Snow possible" thresholds of Haynes et al. (2009). In the near-surface bin, the observed reflectivity is corrected for path integrated gaseous and hydrometeor attenuation, then compared to the threshold. Gaseous attenuation is obtained from the 2B-GEOPROF Gaseous_attenuation variable, and hydrometeor attenuation from the 2C-PRECIP-COLUMN PIA_near_surface variable. If the corrected reflectivity in the near-surface bin exceeds the threshold, an upward search is made for the precipitation echo top. Since path integrated hydrometeor attenuation estimates are not available for range bins above the near-surface bin, the reflectivity profile above the near-surface bin is corrected only for gaseous attenuation. The precipitation echo top is identified in the last range bin for which the corrected reflectivity exceeds the -15 dBZe threshold. The contiguous layer from the near-surface bin to the precipitation echo top is identified as a precipitation layer.

Finally, temperatures in the precipitation layer are examined to determine whether frozen precipitation is present. Using the ECMWF-AUX Temperature variable, if all temperatures are below 0° C, the entire precipitation layer is identified as a snow layer. Otherwise, a search is made to find the contiguous frozen layer at the base of the precipitation layer. If such a layer is found, it is identifed as a snow layer.

4.1.3 Surface precipitation characterization

An initial evaluation for snow at the surface is done using the 2C-PRECIP-COLUMN variables Precip_flag and Melted_fraction. If Precip_flag has a value of 4 ("snow possible") or 5 ("snow certain"), 2C-SNOW-PROFILE indicates snow at the surface. If Precip_flag has a value of 6 ("mixed possible") or 7 ("mixed certain"), the value of Melted_fraction is examined. If Melted_fraction <= 0.1, 2C-SNOW-PROFILE also indicates snow at the surface. If the value of Precip_flag is missing, or if Precip_flag indicates mixed phase precipitation but Melted_fraction is missing, this state triggers a further attempt by the 2C-SNOW-PROFILE algorithm to evaluate the surface precipitation type.

If mixed phase precipitation is occurring but the melted fraction is unknown, the scene characterization will attempt to determine the melting depth (distance from the surface to the melting level) using the ECMWF-AUX temperature profile. If the melting depth is shallow, such that the melted mass fraction is expected to be less than 0.1, the surface precipitation is considered to be snow. Using the results of the melting layer model of Haynes et al. (2009), the maximum allowed melting depth for a melted mass fraction of 0.1 is 240 m. With an assumed environmental lapse rate of 6° C km^{-1}, this approach is equivalent to assuming snow exists at temperatures up to 1.5° C. A similar threshold (2° C) was found by Liu (2008) based on an analysis of present weather reports from shipboard and land station observations.

If the value of Precip_flag is missing, but the profile characterization identified a snow layer, the scene characterization will again attempt to determine the melting depth using the ECMWF-AUX temperature profile. If the melting depth is less than the threshold of 240 m, the surface precipitation is again considered to be snow.

4.2 Optimal estimation retrieval

The optimal estimation method for 2C-SNOW-PROFILE works by minimizing a cost function which represents differences between simulated and observed reflectivities and also differences between estimated and a priori values for the snow microphysical properties (Rodgers, 2000). Given a vector of reflectivity observations y and a state vector x of unknown microphysical properties to be retrieved, a corresponding reflectivity forward model $F(x,\tilde{b})$ is constructed which relates x and y. The forward model may require other parameters, $\tilde{b}$, not to be retrieved, where the tilde indicates that these parameters may be known imperfectly. The forward model is typically an approximation of the true physical relation between x and y, and there are uncertainties associated with both the reflectivity observations y and the parameters $\tilde{b}$. Allowing for these uncertainties gives the statement of the forward problem:

$$y = F(x,\tilde{b}) + \varepsilon, \tag{10}$$

where ε represents the total uncertainty, due both to measurement uncertainty and to uncertainties in the forward model. These uncertainties may be due to both systematic and random errors.

It is desired to find the state $\hat{x}$ which maximizes the posterior conditional probability density function (PDF) $P(x \mid y)$, subject also to prior knowledge about the values of $x\}$. This prior knowledge is described by expected values x_a and their covariances $\mathbf{S}_a$. The posterior PDF is evaluated by constructing the cost function

$$\Phi(x,y,x_a) = \left(y - F(x,\tilde{b})\right)^{\mathsf{T}} \mathbf{S}_\varepsilon^{-1} \left(y - F(x,\tilde{b})\right) + (x - x_a)^{\mathsf{T}} \mathbf{S}_a^{-1} (x - x_a), \tag{11}$$

and minimizing with respect to x, where $\mathbf{S}_\varepsilon$ is the covariance matrix representing the uncertainties $\boldsymbol{\varepsilon}$. If $\boldsymbol{\varepsilon}$ contains systematic errors which can be identified, it is desirable to correct for them by adjusting the model or measurements and determining a corrected $\mathbf{S}_\varepsilon$ (Marks and Rodger, 1993).

Provided the forward model is not excessively nonlinear, the vector $\hat{x}$ which minimizes the cost function can be found by Newtonian iteration:

$$\hat{x}_{i+1} = \hat{x}_i + \left(\mathbf{S}_a^{-1} + \mathbf{K}_i^{\mathsf{T}} \mathbf{S}_\varepsilon^{-1} \mathbf{K}_i\right)^{-1} \left[\mathbf{K}_i^{\mathsf{T}} \mathbf{S}_\varepsilon^{-1} \left(y - F(\hat{x}_i,\tilde{b})\right) - \mathbf{S}_a^{-1} (\hat{x}_i - x_a)\right], \tag{12}$$

where $\mathbf{K}$ is the Jacobian of the forward model with respect to the state vector, and $\mathbf{K}_i = \mathbf{K}(\hat{x}_i)$. Iteration continues until the covariance-weighted difference in successive state vector estimates is much smaller than the number of state vector elements. At convergence, the covariance of the solution $\hat{x}$ is obtained as

$$\hat{\mathbf{S}}_x = \left(\hat{\mathbf{K}}^{\mathsf{T}} \mathbf{S}_\varepsilon^{-1} \hat{\mathbf{K}} + \mathbf{S}_a^{-1}\right)^{-1}, \tag{13}$$

where $\hat{\mathbf{K}} = \mathbf{K}(\hat{x})$. As a diagnostic test of the results, a χ^2 statistic is calculated using the retrieved state vector in (11). A value near N_y, the number of observations, suggests correct convergence.

The observation vector for this retrieval is the vertical profile of reflectivities observed by CloudSat, corrected for gaseous attenuation,

$$y = \begin{bmatrix} Ze_1 \\ \vdots \\ Ze_{N_y} \end{bmatrix} \tag{14}$$

where N_y is the number of radar range bins in the snow layer. Because of the large range of Ze, the values used for the retrieval are in decibels.

The state at each radar bin is described by the exponential size distribution parameters N_0 and λ. Values for N_0 may range over several orders of magnitude, so $\log(N_0)$ is retrieved instead. The variability of λ is significantly smaller than that of N_0; however, examination of fitted exponential distributions from C3VP snow events showed that the distribution of values for λ was strongly non-Gaussian. The log-transformed values are much less skewed, and accordingly, $\log(\lambda)$ is retrieved instead. The corresponding state vector to be retrieved is then

$$\hat{x} = \begin{bmatrix} \log(N_0)_1 \\ \vdots \\ \log(N_0)_{N_y} \\ \log(\lambda)_1 \\ \vdots \\ \log(\lambda)_{N_y} \end{bmatrix}. \tag{15}$$

and the associated covariance matrix is

$$\hat{\mathbf{S}}_x = \begin{bmatrix} s^2\left(\log\left(N_0\right)_1\right) & \cdots & \cdots & s\left(\log\left(N_0\right)_1, \log\left(\lambda\right)_{N_y}\right) \\ & \ddots & & \\ \vdots & s^2\left(\log\left(N_0\right)_{N_y}\right) & & \vdots \\ \vdots & & s^2\left(\log\left(\lambda\right)_1\right) & \vdots \\ & & & \ddots \\ s\left(\log\left(N_0\right)_1, \log\left(\lambda\right)_{N_y}\right) & \cdots & \cdots & s^2\left(\log\left(\lambda\right)_{N_y}\right) \end{bmatrix}. \tag{16}$$

4.2.1 Radar forward model

Following the reasoning described in the discussion of multiple scattering and attenuation, both the singly-scattered attenuated and nonattenuated reflectivities are modeled. Applying the exponential distribution with (1) and omitting the attenuation term, the singly-scattered nonattenuated reflectivity $Ze^{ss,na}$ at range bin i is

$$Ze^{ss,na}\left(N_{0,i};\lambda_i;\tilde{b}_i\right) = \frac{\Lambda^4}{\|K_w\|^2 \pi^5} \int_{D_{M,min}}^{D_{M,max}} N_{0,i} \exp\left(-\lambda_i D_M\right) \sigma_{bk}(D_M, \tilde{b}_i)\, dD_M. \tag{17}$$

The backscatter cross-section σ_{bk} has been written to show its dependence on a vector of parameters $\tilde{b}_i$ as well as on D_M. The vector $\tilde{b}_i$ includes the parameters for the mass- and area-dimension relations α, β, γ, and σ which were used to construct the particle models from which the scattering properties were calculated. The tilde indicates that these parameters are approximations of the true values. Following (1) and (2), the singly-scattered attenuated reflectivity $Ze^{ss,a}$ is

$$Ze^{ss,a}\left(N_{0,i};\lambda_i;\tilde{b}_i;R_i\right) \quad = \quad Ze^{ss,na}\left(N_{0,i};\lambda_i;\tilde{b}_i\right)\left(\mathscr{T}\left(R_{0,i}\right)\right)^2 \tag{18}$$

where $R_{0,i}$ is the range to bin i and $\mathscr{T}$ is the one-way transmission to the radar bin:

$$\mathscr{T}\left(R_{0.i}\right) = \mathscr{T}_{0,i} = \exp\left[-\int_{s=0}^{s=R_{0,i}} \beta_{ext}(s)\, ds\right]. \tag{19}$$

Since reflectivities have been corrected for gaseous attenuation, the volume extinction coefficient β_{ext} is

$$\beta_{ext}(s) = \int_{D_{M,min}}^{D_{M,max}} N_0(s) \exp\left(-\lambda(s) D_M\right) \sigma_{ext}(D_M, \tilde{b}(s))\, dD_M. \tag{20}$$

The dependence of $\mathscr{T}$ on the vertical profile of N_0 and λ has been omitted from the notation for clarity.

The results of Matrosov and Battaglia (2009) shown in their Figure 3 suggest that the multiply-scattered attenuated reflectivity $Ze^{ma,a}$ falls approximately midway between $Ze^{ss,a}$ and $Ze^{ss,na}$ in decibel units. Accordingly $Ze^{ms,a}$ at radar bin i is approximated as the geometric mean of the two singly-scattered reflectivities in linear units,

$$\begin{aligned} Ze_i^{ms,a} \quad &\approx \quad \left[Ze_i^{ss,na} Ze_i^{ss,a}\right]^{1/2} \\ &\approx \quad Ze_i^{ss,na}\, \mathscr{T}_{0,i}. \end{aligned} \tag{21}$$

The vector F of forward modeled reflectivities is then

$$F = \begin{bmatrix} dBZe_1^{ms,a} \\ \vdots \\ dBZe_{N_y}^{ms,a} \end{bmatrix} = \begin{bmatrix} Ze_1^{ss,na}\, \mathscr{T}_{0,1} \\ \vdots \\ Ze_{N_y}^{ss,na}\, \mathscr{T}_{0,N_y} \end{bmatrix} \tag{22}$$

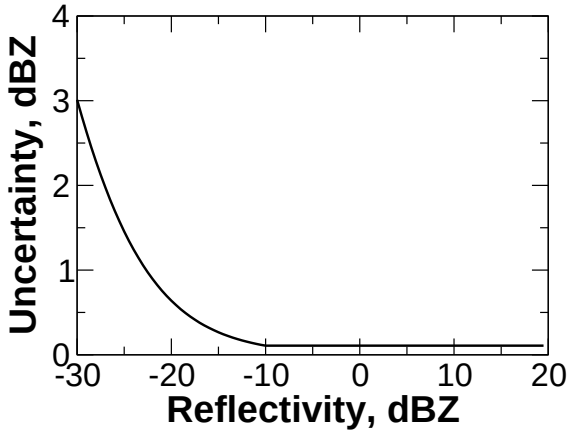

Figure 1: Upward uncertainty based on one standard deviation of noise for the CloudSat CPR.

or, in decibel units,

$$F = \begin{bmatrix} dBZe_1^{ss,na} + dB\mathscr{T}_{0,1} \\ \vdots \\ dBZe_{N_y}^{ss,na} + dB\mathscr{T}_{0,N_y} \end{bmatrix} \tag{23}$$

where $dB\mathscr{T}_{0,i} = 10\log(\mathscr{T}_{0,i})$. This approach amounts to an estimated bias correction applied to the singly-scattered nonattenuated reflectivities $dBZe_i^{ss,na}$.

4.2.2 Measurement and forward model uncertainties

The error covariance matrix $\mathbf{S}_\varepsilon$ describes the uncertainties associated with model-measurement differences for the CloudSat retrieval and is composed of two terms:

$$\mathbf{S}_\varepsilon = \mathbf{S}_y + \mathbf{S}_F \tag{24}$$

where $\mathbf{S}_y$ is the covariance matrix describing the measurement uncertainties and $\mathbf{S}_F$ is the forward model error covariance matrix.

The sources of measurement uncertainty include uncertainty in the absolute radiometric calibration and measurement noise. The noise characteristics of the CPR vary with signal strength. For reflectivities above -10 dBZ, one standard deviation of noise as a fraction of the mean signal is about -16 dB, while for reflectivities below -10 dBZ, noise is an increasing fraction of the signal, reaching 0 dB at the minimum detectable signal of -30 dBZ (R. Austin, personal communication, 4 November, 2008). The resulting uncertainties range from 3 dBZ for a reflectivity of -30 dBZ to about 0.1 dBZ for reflectivities above -10 dBZe. (Figure 1). Calibration errors, which would result in a bias in the measured reflectivities, are expected to be less than 2 dB based on a prelaunch calibration error budget (Tanelli et al., 2008), but the value of this bias is unknown and isn't considered. To construct $\mathbf{S}_y$, variances for each range bin are computed as the squares of these uncertainties and uncertainties in distinct range bins are considered to be uncorrelated, resulting in a diagonal form for $\mathbf{S}_y$.

Several sources contribute to the forward model uncertainties represented by $\mathbf{S}_F$. A complete description of the methods used to assess these sources and the resulting uncertainties can be found in (Wood, 2011). Briefly, the forward-modeled reflectivities have uncertainties due to two sources: first, the approximate nature of the transmission-based bias correction for multiple scatterng and attenuation given in (21); and second, the uncertainties in the singly-scattered nonattenuated reflectivities given in (17). For the first source, the values of $Ze^{ss,na}$ and $Ze^{ss,a}$ place upper and lower bounds on the expected value of $Ze^{ms,a}$ and can be used to make a rudimentary estimate of this uncertainty. The estimate used here is that the uncertainty in $Ze^{ms,a}$ is one-half the

difference between $Ze^{ms,a}$ and $Ze^{ss,na}$ in decibels. The resulting estimate of the variance at each radar bin is then

$$\begin{aligned} s^2\left(dBZe_i^{ms,a}\right) &= \left[\frac{1}{2}\left(dBZe_i^{ss,na} - dBZe_i^{ms,a}\right)\right]^2 \\ &= \left[\frac{1}{2} dB\mathscr{T}_{0,i}\right]^2. \end{aligned} \tag{25}$$

This simple approach is not sufficient to diagnose vertical correlations in these uncertainties, so covariances between radar bins are set to zero so that the resulting covariance matrix is diagonal.

For the second source, the uncertainties may be further decomposed as the sum of two terms: $\mathbf{S}_B^{ss,na}$, which is a covariance matrix describing uncertainties due to the forward model parameters $\tilde{b}$, and $\mathbf{S}_F^{ss,na}$, which is a covariance matrix describing uncertainties due to other assumptions in the calculation of $Ze^{ss,na}$. $\mathbf{S}_B^{ss,na}$ is calculated as

$$\mathbf{S}_B^{ss,na} = \mathbf{K}_b \mathbf{S}_b \mathbf{K}_b^{\mathsf{T}} \tag{26}$$

where $\mathbf{K}_b$ is the Jacobian of the forward model reflectivities with respect to the parameters $\tilde{b}$ and $\mathbf{S}_b$ is the covariance matrix for the parameters. Per (17), $\tilde{b}$ includes the microphysical parameters α, β, γ, and σ used to construct the particle models and calculate scattering properties. $\mathbf{K}_b$ depends on the estimated state $\hat{x}$ and so is evaluated at each iterative step using a set of perturbed particle models. In general, $\mathbf{S}_B^{ss,na}$ is not diagonal, because attenuation causes reflectivities in the profile to be dependent on the state of radar bins at higher altitudes and so $\mathbf{K}_b$ is not diagonal.

The forward modeled reflectivities depend on other assumptions whose contributions to uncertainties are quantified in $\mathbf{S}_F^{ss,na}$. These sources include the choice of particle shape, the placement of dipoles in the DDA models, discretization and truncation of the integrations over size distribution, and the assumption of the exponential distribution. Analyses using alternate DDA dipole models and observed particle size distributions provided estimates for these terms, which are expected to be uncorrelated with each other and with uncertainties in adjacent radar bins, giving $\mathbf{S}_F^{ss,na}$ diagonal form.

4.2.3 A priori estimates of the state

For each profile, the a priori state consists of a vector of expected values x_a and the corresponding covariance matrix $\mathbf{S}_a$, having the same sizes as the state vector x (15) and its covariance matrix $\mathbf{S}_x$ (16). A priori estimates of $\log(N_0)$ and $\log(\lambda)$ at each bin of the snow layer are determined using temperature-based parameterizations derived from snow PSDs observed during C3VP and in conjunction with PSDs from other field experiments (Wood, 2011). Values vary through the profile depending on the temperatures in the ECMWF-AUX product. Uncertainties in the values arise because of natural variability and errors in the observations, and were estimated using the residual standard deviations between the parameterized and observed values. The uncertainty model also includes covariance between $\log(N_0)$ and $\log(\lambda)$ within each radar bin, as indicated by the analyzed observations, giving $\mathbf{S}_a$ a tridiagonal form. For the retrieval iterations, the a priori covariance matrix is scaled to larger values to allow the a priori state to stabilize the retrieval without causing bias. The unscaled covariance matrix is then used to estimate the uncertainties in the retrieved state.

4.3 Derived products: Snowfall rate and snow water content

Provided a retrieval is successful, snowfall rates are calculated as described in Section 3.2 from the retrieval results for each radar bin in the snow layer. Uncertainties for snowfall rate are determined in a manner similar to that used for the forward model uncertainties. The total uncertainty is decomposed into terms due to 1) uncertainties in the retrieved state, 2) uncertainties in the particle model parameters, 3) uncertainties in the fallspeed model, and 4) uncertainties associated with the assumed exponential distribution. These terms are evaluated using the covariance matrix for the retrieved state, $\hat{\mathbf{S}}_x$ as well as the results from several other analyses as described in Wood (2011). Snow water contents are calculated analogously as

$$SWC(R) = \int_{D_{min}}^{D_{max}} N(D,R) m(D,R)\, dD, \tag{27}$$

along with uncertainties. The surface snowfall rate and its uncertainty are taken to be equal to the values at the base of the snow layer.

5 Algorithm Inputs

The algorithm uses inputs from the 1B-CPR, 2B-GEOPROF, 2C-PRECIP-COLUMN and ECMWF-AUX products (Table 5).

Table 5: 2C-SNOW-PROFILE inputs.

Source	Name	Dimension	Units
1B-CPR	RayHeader_RangeBinSize	scalar	m
2B-GEOPROF	TAI_start	scalar	seconds
"	Latitude	N_{ray}	degrees
"	Longitude	N_{ray}	degrees
"	Height	N_{bin},N_{ray}	m
"	DEM_elevation	N_{ray}	m
"	Vertical_binsize	scalar	m
"	SurfaceHeightBin	N_{ray}	–
"	CPR_Cloud_mask	N_{bin},N_{ray}	–
"	Gaseous_Attenuation	N_{bin},N_{ray}	dB
"	Radar_Reflectivity	N_{bin},N_{ray}	dBZe
2C-PRECIP-COLUMN	Precip_flag	N_{ray}	–
"	Melted_fraction	N_{ray}	–
"	Surface_type	N_{ray}	–
"	PIA_near_surface	N_{ray}	dB
ECMWF-AUX	Temperature	N_{bin},N_{ray}	K
"	Pressure	N_{bin},N_{ray}	Pa

6 2C-SNOW-PROFILE output file data structure

Table 6 summarizes the output file data structure.

Table 6: 2C-SNOW-PROFILE output file data structure

Data Granule			Variable Name	Dimension	Units
	Swath Data	Geolocation Fields	Profile_time	N_{ray}	seconds
			UTC_start	scalar	seconds
			TAI_start	scalar	seconds
			Latitude	N_{ray}	degrees
			Longitude	N_{ray}	degrees
			Height	N_{ray}	m
			DEM_elevation	N_{ray}	m
			Vertical_binsize	scalar	m
		2B-GEOPROF pass-through fields	Data_quality	N_{ray}	–
			Data_status	N_{ray}	–
			Data_targetID	N_{ray}	–
		2C-SNOW-PROFILE data fields	snow_retrieval_status	N_{ray}	–
			norm_chi_square	N_{ray}	–
			snowfall_rate	N_{bin},N_{ray}	mm h^{-1}
			snowfall_rate_uncert	N_{bin},N_{ray}	mm h^{-1}
			log_N0	N_{bin},N_{ray}	$\log_{10}(m^{-3}mm^{-1})$
			log_N0_uncert	N_{bin},N_{ray}	$\log_{10}(m^{-3}mm^{-1})$
			log_lambda	N_{bin},N_{ray}	$\log_{10}(mm^{-1})$
			log_lambda_uncert	N_{bin},N_{ray}	$\log_{10}(mm^{-1})$
			snowfall_rate_sfc	N_{ray}	mm h^{-1}
			snowfall_rate_sfc_uncert	N_{ray}	mm h^{-1}
			snowfall_rate_sfc_confidence	N_{ray}	–
			snow_water_content	N_{bin},N_{ray}	g m^{-3}
			snow_water_content_uncert	N_{bin},N_{ray}	g m^{-3}

7 Retrieval Example

Figure 2 provides an example of a snowfall scene from granule 3451 and the corresponding retrieval results. Over land surfaces such as this, the near-surface bin is placed at the 5th bin above the bin containing the surface. For some profiles in the southern portion of this scene, although significant reflectivity is present in the near-surface bin, the reflectivity does not meet the precipitation threshold and no retrieval is performed. For profiles in the northern portion of the scene, the near-surface bin does not contain significant reflectivities.

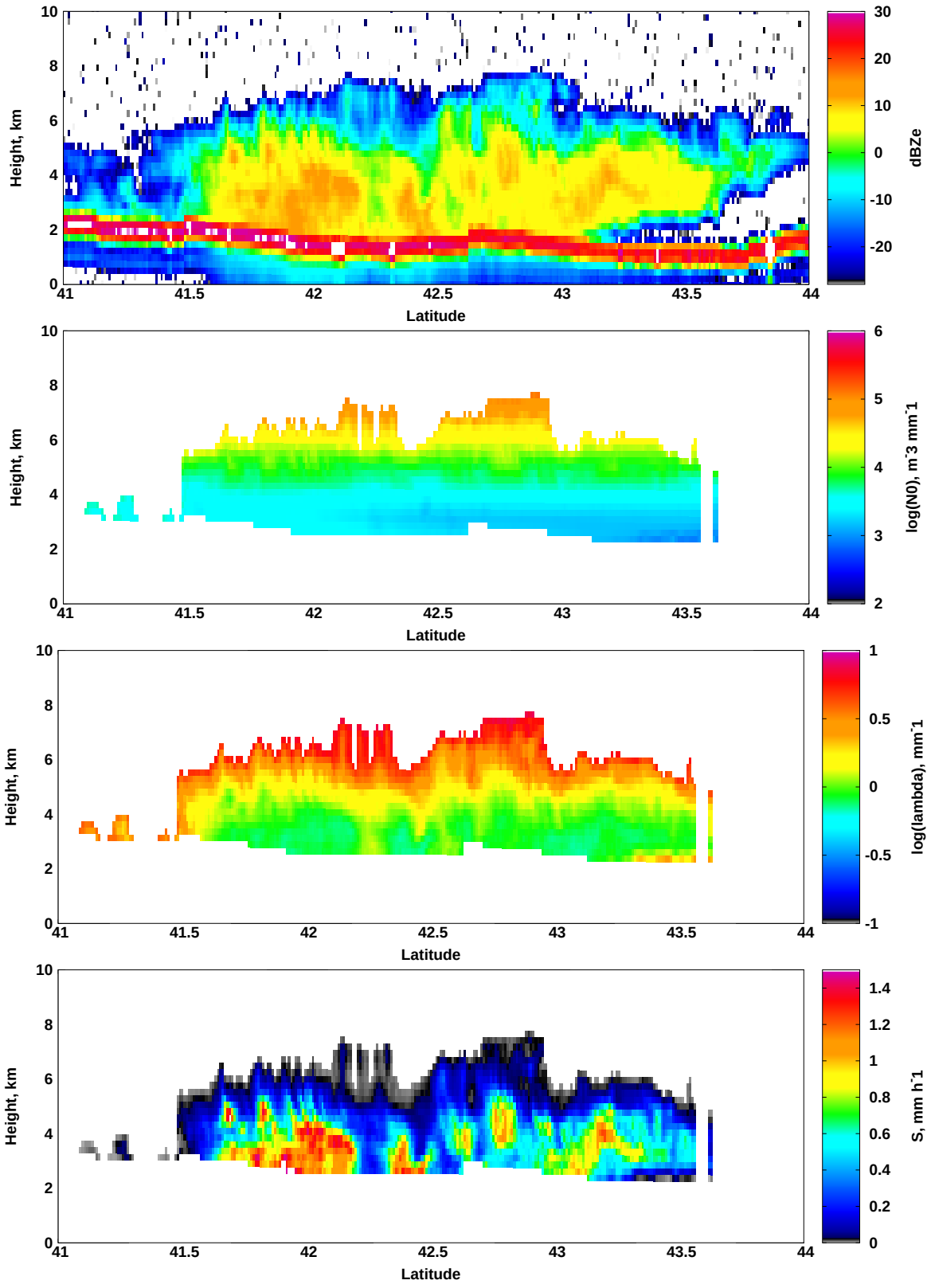

Figure 2: Retrieval example from granule 3451, showing (from top to bottom) the reflectivity field from 2B-GEOPROF, the retrieved values of $\log(N_0)$and $\log(\lambda)$, and the resulting snowfall rates calculated from the retrieved values.

8 Caveats and Known Issues

Retrieval status bit 3 Bit 3 of snow_retrieval_status is set when the snowfall rate in the near-surface bin is substantially different from that in the bin immediately above. This situation may arise in several different scenarios. First, for steeply-varying terrain, it's presently unclear whether placing the near-surface bin in the 5th bin above the surface is sufficient to eliminate the effects of ground clutter on retrievals for snow scenes. Ground clutter effects in this bin have the potential to cause the retrieval to produce anomalously high snowfall rates which would likely not be present in the bin above. Second, partial melting of snow particles may enhance radar reflectivity. The forward model used by the retrieval assumes dry snow properties. To reproduce the enhanced reflectivity, the retrieval would likely overestimate snowfall rate in the bin containing the melted particles. Finally, shallow precipitation might lead to a significant snowfall rate in the near-surface bin with none in the bin above.

Two separate criteria are used to set bit 3. First, in scenes for which the near-surface bin is the only bin in the snow layer, bit 3 is set if the snowfall rate in the near-surface bin exceeds 5 mm h^{-1}. This threshold was determined based on an evaluation of the distribution of retrieved snowfall rates under this scenario, which showed a bimodal distribution with a minimum at approximately 5 mm h^{-1}. Second, if the near-surface bin and the bin immediately above both contain snow, bit 3 is set if the ratio of the snowfall rate in the lower bin to that in the upper bin exceeds a threshold based on the snowfall rate in the upper bin. This threshold was determined by comparing distributions of these ratios with distributions of corresponding ratios from bins slightly higher in the retrieved profiles.

Users should evaluate whether the flagged profiles are of concern for their analyses. In situations where the users conclude the flagged profiles may be affected by ground clutter, retrieval results for the bin above the near-surface bin may be used to estimate the surface snowfall rate; however, since each retrieval is performed on the snow layer as a whole, the results in distinct bins are not fully independent.

9 Operator Instructions

The 2C-SNOW-PROFILE algorithm operates as part of the CloudSat Operational and Research Environment (CORE). For each processed granule, the algorithm produces a metadata file at the conclusion of processing. The metadata contains counts of the number of profiles classified as having snow or predominantly frozen mixed-phase precipitation at the surface, along with counts profiles with failed retrievals or with data insufficient for the retrieval to run. Additionally, the metadata contains a histogram of surface snowfall rates.

Bibliography

Abraham, F. F., 1970: Functional dependence of drag coefficient of a sphere on Reynolds number. *Phys. Fluids*, **13**, 2194-2195.

Braham, R. R., Jr., 1990: Snow particle spectra in lake effect snows. *J. Appl. Meteorol.*, **29**, 200-207.

Brandes, E. A., K. Ikeda, G. Zhang, M. Schoenhuber, and R. M. Rasmussen, 2007: A statistical and physical description of hydrometeor distributions in Colorado snowstorms using a video disdrometer. *J. Appl. Meteorol. Clim.*, **46**, 634-650, doi:10:1175/JAM2489.1.

Draine, B. T., and P. J. Flatau, 1994: Discrete-dipole approximation for scattering calculations. *J. Opt. Soc. Am. A*, **11**, 1491-1499.

Gordon, G. L., and J. D. Marwitz, 1984: An airborne comparison of three PMS probes. *J. Atmos. Ocean. Tech.,* **1**, 22-27.

Haynes, J. M., T. S. L'Ecuyer, G. L. Stephens, S. D. Miller, C. Mitrescu, N. B. Wood, and S. Tanelli, 2009: Rainfall retrieval over the ocean with spaceborne W-band radar. *J. Geophys. Res.*, **114**, D00A22, doi:10.1029/2008JD009973.

Herzegh, P. H., and P. V. Hobbs, 1985: Size spectra of ice particles in frontal clouds: correlations between spectrum shape and cloud conditions. *Q. J. Roy. Meteor. Soc.*, **111**, 463-477.

Heymsfield, A. J., P. Field, and A. Bansemer, 2008: Exponential size distribution for snow. *J. Atmos. Sci.*, **65**, 4017- 4031, doi:10.1175/2008JAS2583.1.

Houze, R. A., Jr., P. V. Hobbs, P. H. Herzegh, and D. B. Parsons, 1979: Size distributions of precipitation particles in frontal clouds. *J. Atmos. Sci.*, **36**, 156-162.

Hudak, D., H. Barker, P. Rodriguez, and D. Donovan, 2006: The Canadian CloudSat validation project. *Proc. Fourth European Conf. on Radar in Hydrology and Meteorology*, Barcelona, Spain, 609-612. [Available online at `http://www.erad2006.org/`].

Liu, G., 2008: Deriving snow cloud characteristics from CloudSat observations. *J. Geophys. Res.*, **113**, D00A09, doi:10.1029/2007JD009766.

Lo, K. Kenneth, and R. E. Passarelli, Jr., 1982: The growth of snow in winter storms: An airborne observational study. *J. Atmos. Sci.*, **39**, 697-706.

Locatelli, J. D. and P. V. Hobbs, 1974: Fall speeds and masses of solid precipitation particles. *J. Geophys. Res.*, **79**, 2185-2197.

Marks, C. J. and C. D. Rodgers, 1993: A retrieval method for atmospheric composition from limb emission measurements. *J. Geophys. Res.*, **98**, 14939-14953.

Matrosov, S. Y., and A. Battaglia, 2009: Influence of multiple scattering on CloudSat measurements in snow: A model study. *Geophys. Res. Lett.*, **36**, L12806, doi:10.1029/2009GL038704.

Mitchell, D. L., 1996: Use of mass- and area-dimensional power laws for determining precipitation particle terminal velocities, *J. Atmos. Sci.*, **53**, 1710-1723.

Mitchell, D. L., and A. J. Heymsfield, 2005: Refinements in the treatment of ice particle terminal velocities, highlighting aggregates. *J. Atmos. Sci.*, **62**, 1637-1644.

Passarelli, R. E., Jr., 1978: Theorectical and observational study of snow-size spectra and snowflake aggregation efficiencies. *J. Atmos. Sci.*, **35**, 882-889.

Rodgers, C., 2000: *Inverse methods for atmospheric sounding*, World Scientific Publishing, Singapore. 240 pp.

Rogers, D. C., 1973: The aggregation of natural ice crystals. M. S. thesis, University of Wyoming, 91 pp.

Stephens, G. L., and N. B. Wood, 2007: Properties of tropical convection observed by millimeter-wave radar systems. *Mon. Weather Rev.*, **135**, 821-842, doi:10.1175/MWR3321.1.

Stephens, G. L., and coauthors, 2002: The CloudSat mission and the A-train: A new dimension of space-based observations of clouds and precipitation. *B. Am. Meteorol. Soc.*, **83**, 1771-1790.

Tanelli, S., S. L. Durden, E. Im, K. S. Pak, D. G. Reinke, P. Partain, J. M. Haynes, and R. T. Marchand, 2008: CloudSat's cloud profiling radar after two years in orbit: Performance, calibration and processing. *IEEE. T. Geosci. Remote*, **46**, 3560-3573.

Wood, N. B., 2011: Estimation of snow microphysical properties with application to millimeter-wavelength radar retrievals for snowfall rate. Ph.D. dissertation, Colorado State University, 248 pp. [Available from Colorado State University, Digital Collections, `http://hdl.handle.net/10217/48170`].

Woods, C. P., M. T. Stoelinga, and J. D. Locatelli, 2008: Size spectra of snow particles measured in wintertime precipitation in the Pacific Northwest. *J. Atmos. Sci.*, **65**, 189-205, doi:10.1175/2007JAS2243.1.